Surface Science 253 (1991) 334–344
North-Holland

EAM study of surface self-diffusion of single adatoms of fcc metals Ni, Cu, Al, Ag, Au, Pd, and Pt

C.L. Liu [a], J.M. Cohen [b], J.B. Adams [a] and A.F. Voter [b]

[a] *Department of Materials Science and Engineering, University of Illinois at Urbana-Champaign, Urbana, IL 61801, USA*
[b] *Theoretical Division, T-12, MS-B268, Los Alamos National Laboratory, Los Alamos, NM 87545, USA*

Received 27 December 1990; accepted for publication 7 February 1991

Self-diffusion of single adatoms on the (100), (110), (111), (311), and (331) surfaces of fcc metals is investigated with the embedded atom method (EAM). The general trend of activation energies for these surfaces is consistent with experimental observations. The calculated activation energies for Ni are in excellent agreement with experimental data, but those for Al and Pt differ from experimental values by up to a factor of 3. The estimated pre-exponential factors are in the range of 10^{-4}–10^{-2} cm^2/s, in good agreement with experiment.

1. Introduction

Diffusion of single adatoms on metal surfaces is important in understanding surface-related phenomena, such as thin-film and crystal growth, sintering, corrosion, and surface chemical reactions. A major tool for investigating surface diffusion is the field ion microscope (FIM), since it is capable of resolving individual atoms. The first comprehensive surface diffusion study utilizing FIM was reported by Ehrlich and Hudda [1]. Following their pioneering work many extensive FIM experiments were carried out. These efforts have been primarily limited to a few metals: tungsten [1–6], rhodium [7], platinum [8,9], nickel [10], and iridium [2,8,11–14]. Some data on the self-diffusion of single aluminum adatoms have been obtained by measuring the onset temperatures at which surface diffusion begins [15].

In general, FIM experiments determine the diffusion constant (D) of single adatoms at several temperatures and fit the results to an Arrhenius form,

$$D = D_0 \exp(-E_d/k_B T), \quad (1)$$

where E_d is the activation energy, D_0 is the pre-exponential factor, and k_B is the Boltzmann factor. The experiments are usually restricted to a narrow temperature range. Below this range no discernable diffusion occurs, while above it the diffusion rate is too high to be measured (adatoms pass beyond the edge of the narrow FIM tips). Thus, small error bars in D can result in large error bars in E_d and D_0. For example, experimental D_0 values for the diffusion of impurities on the W(211) surface have ranged over five orders of magnitude. However, a recent study by Wang and Ehrlich [16] showed that experiments with better statistics yielded a much smaller variation in D_0 (only one order of magnitude). Typical values of the pre-exponential factor were in the neighborhood of 10^{-3} cm^2/s.

Many theoretical studies of diffusion on metal surfaces have been carried out [17,18]. Most of these involved the use of Morse or Lennard-Jones potentials. These results are not usually satisfactory. For example, calculations with Morse potentials yielded reasonable values of activation energies for Pt and Rh, but very poor data for Ni [17].

The purpose of the present paper is to determine if the new many-body potentials are more reliable for surface diffusion studies. The chosen potentials were derived from the embedded atom

method (EAM) developed by Daw and Baskes [19]. Previous work with the EAM potentials has shown impressive agreement between calculated and experimental properties of fcc metals [20,21], including bulk diffusion [22] and surface structure [23]. The EAM has been applied to self-diffusion on the Ag(100) surface [24,25], but no experimental data are available for comparison.

This paper offers the results of a comprehensive study of surface self-diffusion of single adatoms on seven fcc metals using two different sets of EAM potentials. These results are compared with all of the available FIM data. Section 2 briefly discusses the EAM and section 3 outlines the computational procedures. The results are given in section 4. The conclusions appear in the final section.

2. The embedded atom method

The EAM is a model developed by Daw and Baskes [19] for calculating the total energy of an arbitrary arrangement of atoms in a metal. It is based on density functional theory, which asserts that the energy of a solid can be written as a unique functional of the electron density distribution. In the EAM this is assumed to be the local density at each atomic site. This energy is further divided into an electrostatic pair interaction plus an embedding energy. Thus, the total energy of an arbitrary arrangement of atoms is given by

$$E_{\mathrm{tot}} = \sum_i F(\rho_i) + \tfrac{1}{2} \sum_{\substack{i,j \\ (i \neq j)}} \Phi(R_{ij}). \tag{2}$$

Here, $F(\rho)$ is the embedding energy, ρ is the local electron density, $\Phi(R)$ is the short-range electrostatic interaction, and R is the distance between atoms. The sums in eq. (2) are over all atoms. This form of potential is also known as the second moment model [26] and the glue model [27].

The EAM functions were determined empirically by fitting to several measured properties, namely: the equilibrium lattice constants, sublimation energy, bulk modulus, elastic constants, and vacancy formation energy. For this study we have used two different sets of EAM functions. One set of functions (AFW) was developed by Adams, Foiles and Wolfer [22]. These functions are nearly identical to the standard ones developed by Foiles, Baskes and Daw (FBD) [28], but they are fit to more accurate estimates of the vacancy formation energy. The Al functions for the AFW set are taken from Foiles and Daw [29]. The second set of functions (VC) was developed by Voter [24,30] and Voter and Chen [31]. The primary difference between the VC potentials and the AFW potentials is that the experimental properties used in the fit included diatomic molecular data for the VC potentials. The results obtained from the two sets of EAM functions are listed separately.

3. Computational method

The desired diffusion parameters, E_{d} and D_0, were determined via molecular statics techniques. Using a finite slab of atoms with periodic boundary conditions in the two directions parallel to the surface, two stationary points were found. These points correspond to the adatom at its minimum energy in a binding site and the adatom at the saddle point between two binding sites.

Given the energy of these two configurations, E_{min} and E_{sad}, the diffusion constant in the harmonic approximation is customarily written as [32]

$$D = \frac{n\nu l^2}{2\alpha} \exp\left[\frac{(E_{\mathrm{sad}} - E_{\mathrm{min}})}{k_{\mathrm{B}}T}\right]. \tag{3}$$

In this equation, ν is the attempt frequency (roughly the vibrational frequency of the adatom as discussed below), l is the jump length to an adjacent site, α is the dimensionality of the space ($\alpha = 1$ for a channelled surface, $\alpha = 2$ for typical surface diffusion), and n is the number of jump directions available to the adatom. Implicit in eq. (3) are the assumptions of transition state theory, i.e., that no recrossings or multiple jump events occur – the adatom makes randomly oriented single jumps. Eq. (3) also assumes that the attempt frequency ν is temperature independent, and that quantum mechanical effects are not important. All three of these are good assumptions in the temper-

ature range of the FIM experiments, where the time between adatom jumps is about 1–100 s. At high temperatures, recrossings [33], multiple jumps [34–36], and anharmonic effects [37] can become important, while classical mechanics breaks down at very low temperatures [38]. The desired diffusion parameters are thus

$$E_d = E_{sad} - E_{min}, \quad \text{and} \quad D_0 = \frac{n\nu l^2}{2\alpha}. \tag{4}$$

The computational approach for determining E_{sad}, E_{min}, and ν differed slightly for the AFW and VC potentials. For the AFW potentials, the N-atom slabs were 15 layers thick with roughly 30 atoms per layer and a free surface on two sides. The adatom was moved in steps from one binding site to the adjacent one, allowing all atoms to relax fully to their minimum energy along the $3N-1$ other coordinates at each step. E_{min} and E_{sad} were taken as the minimum and maximum points on the energy–position curve as shown in fig. 1. The attempt frequency was computed from

$$\nu = \frac{1}{2\pi}\sqrt{\frac{c}{m}}, \tag{5}$$

where c is the force constant ($F = -cx$) of a parabola fitted to the region of the curve near E_{min}, and m is the mass of the adatom.

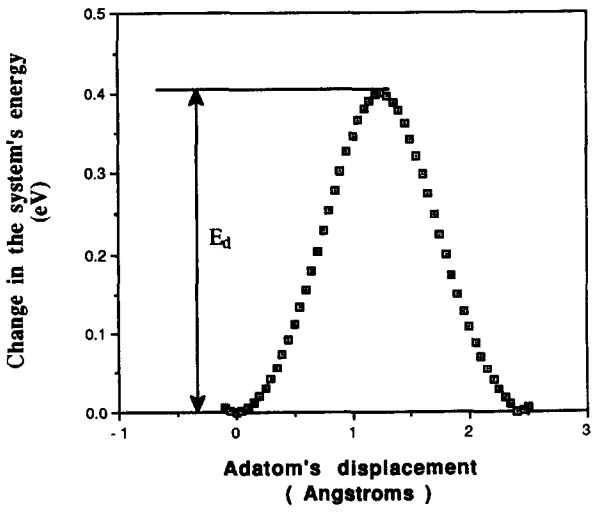

Fig. 1. A typical energy displacement curve for self-diffusion of a Ni adatom on the Ni(110) surface along the surface channel.

For the VC potentials, the slab consisted of an adatom and a number of layers that were free to relax (for a total of N moving atoms) attached to a section of layers frozen at the bulk geometry, so that the slab had one free surface. This approach was also used for the Lennard-Jones calculations and the (110) exchange mechanism using the AFW potentials. The thickness of the frozen section was greater than the cutoff distance for the potential. The number of moving layers and the size of each layer were increased as necessary to achieve convergence of the properties. The minimum and the saddle points were found using a 3-dimensional Newton–Raphson search for the stationary points. The $3N \times 3N$ dynamical matrix was diagonalized to obtain the normal mode frequencies $\{\nu_i\}$ at each stationary point. It was verified that exactly one imaginary frequency existed at the saddle point, while none did at the minimum. Following Vineyard [39], the full harmonic attempt frequency was then determined from the nonimaginary frequencies by

$$\nu = \prod_i^{3N} \nu_i^{min} \Big/ \prod_i^{3N-1} \nu_i^{sad}. \tag{6}$$

Typically, between 2 and 6 free layers were required to achieve convergence of E_d to less than 0.01 eV.

For the (111) surface, which has two slightly different binding sites, the D_0 values in the tables correspond to $T = 0$ K. Adatom memory loss is assumed in the higher energy site.

4. Results and discussion

Surface energies for all of the surfaces considered in this study were determined and the results are listed in table 1. The AFW values are close to those found by Foiles, Baskes and Daw [28] on the (100), (110), and (111) surfaces for Ni, Cu, Ag, Au, Pd, and Pt. Experimental values for the "average" surface [40] are also listed in table 1. The values from the AFW and the VC potentials are about 10–40% lower than the experimental data. Yet, the trend across the elements is good, with the surface energies increasing in the order of Al,

Table 1
Surface energies (ergs/cm^2) at $T = 0$ K calculated using the AFW potentials (upper values) and the VC potentials (lower values) for the surfaces of all the fcc metals examined in the present work. The experimental values are from ref. [40]

Surface	Ni	Cu	Al	Ag	Au	Pd	Pt
(100)	1626	1321	546	703	927	1452	1710
	1755	1330	855	880	891	1641	1549
(110)	1777	1487	585	756	990	1736	1823
	1978	1472	959	967	969	1806	1681
(111)	1492	1215	498	618	797	1300	1606
	1624	1232	824	803	768	1514	1341
(311)	1773	1443	584	759	976	1564	1800
	1973	1466	956	961	954	1797	1658
(331)	1746	1422	577	741	947	1536	1758
	1937	1445	950	945	923	1776	1610
Average face	1638	1378	558	715	927	1518	1739
	1853	1389	909	911	901	1707	1568
Experimental	2380	1790	1140	1250	1510	2000	2490

Ag, Cu, Pd, Ni, and Pt. Additionally, the order of increasing surface energy with respect to crystal face is (111), (100), and (110), which agrees closely with that predicted by Tyson's model [41].

Fig. 2 shows the surface normal views of the five surfaces studied [(100), (110), (111), (311), and (331)]. Besides the standard in-channel diffusion on the (110) surface $\{(110)_{\parallel}\}$, diffusion can occur perpendicular to the channel $\{(110)_{\perp}\}$ via the exchange mechanism shown in fig. 3. An exchange mechanism, depicted in fig. 4, can also operate on the (100) surface $\{(100)_{ex}\}$. Both of these exchange mechanisms are discussed below.

The results of the calculations for the self-diffusion of single adatoms of the fcc metals Ni, Al, Cu, Ag, Au, Pd, and Pt on the (100), (110), (111), (311), and (331) surfaces are displayed in table 2. The experimental data and theoretical values from other models are listed in tables 3 and 4 for comparison. Note that the values for Ni appear

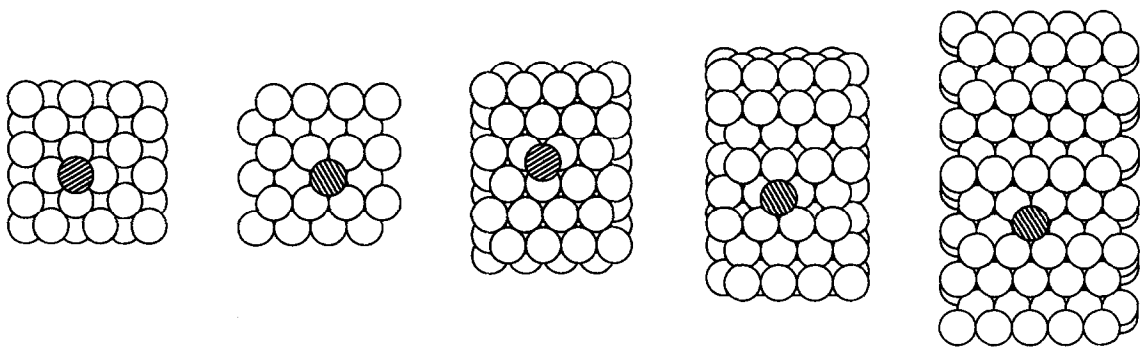

Fig. 2. Top views of the five surfaces considered in the present study. The adatom (shaded) is in the binding site in each case. The values of n and α [eqs. (3) and (4)] are given for the "standard" diffusion mechanism.

separately as table 3, because the experimental data were reanalyzed as discussed in the appendix.

A general trend of activation energies calculated with the EAM potential is found. On the smooth (111) surface (most close-packed) the migration of a single adatom requires a very low activation energy, while the rougher surfaces exhibit higher barriers. Of the five surfaces investigated, the lowest activation energy corresponds to self-diffusion on the (111) surface and the highest on the (100) surface (nonexchange). The calculated activation energies on the (110), (311), and (331) surfaces are similar, particularly on the (110) and (331), as seen in table 2. This can be understood by inspection of fig. 2, which shows that diffusion on fcc(331) is along a tilted (110) facet. The general trend of activation energies across the surfaces discussed above is consistent with the available experimental data, as seen in tables 3 and 4. However, the activation energy on the (111) surface is usually one order of magnitude lower than that on the other surfaces. FIM shows very low values for E_d on Rh(111) (0.16 eV), but a moderate value on Ni(111) (0.33 eV). It should be

Table 2
Activation energy E_d and pre-exponential factor D_0 at T = 0 K calculated using the AFW potentials (upper values) and the VC potentials (lower values) in the present work; E_d is in eV and D_0 is in cm^2/s

Element	(100)	$(100)_{ex}$	$(110)_{\parallel}$	$(110)_{\perp}$	(111)	(311)	(331)
Ni							
E_d	0.63	0.93	0.44	0.49	0.056	0.34	0.45
	0.68	1.15	0.39	0.42	0.063	0.38	0.46
D_0	1.6×10^{-3}		2.3×10^{-3}	3.7×10^{-2}	5×10^{-4}	1.4×10^{-3}	1.4×10^{-3}
	5.4×10^{-3}	4×10^{-2}	4.0×10^{-3}	2.8×10^{-2}	6.2×10^{-4}	4.4×10^{-3}	4.2×10^{-3}
Cu							
E_d	0.38	0.72	0.23	0.30	0.026	0.26	0.28
	0.53	0.79	0.28	0.31	0.044	0.28	0.33
D_0	1.2×10^{-3}		8×10^{-4}	3.2×10^{-2}	3×10^{-4}	1.2×10^{-3}	1.0×10^{-3}
	5.2×10^{-3}	2×10^{-2}	4.4×10^{-3}	2.7×10^{-2}	4.6×10^{-4}	3.1×10^{-3}	3.0×10^{-3}
Al							
E_d	0.40	0.69	0.26	0.30	0.074	0.20	0.27
	0.46	0.25		0.15	0.054	0.24	0.24
D_0	2.0×10^{-3}		1.8×10^{-3}	6.0×10^{-2}	9×10^{-4}	2.0×10^{-3}	2.0×10^{-3}
	1.5×10^{-2}	4×10^{-2}		2.4×10^{-2}	1.6×10^{-3}	6.7×10^{-3}	5.4×10^{-3}
Ag							
E_d	0.48	0.75	0.32	0.42	0.059	0.26	0.34
	0.48	0.60	0.25	0.31	0.044	0.26	0.29
D_0	1.2×10^{-3}		1.0×10^{-3}	4.0×10^{-2}	5×10^{-4}	1.0×10^{-3}	1.0×10^{-3}
	3.9×10^{-3}	2×10^{-2}	2.7×10^{-3}	2.5×10^{-2}	4.1×10^{-4}	3.0×10^{-3}	2.0×10^{-3}
Au							
E_d	0.64	0.30	0.25	0.40	0.021	0.35	0.26
	0.84	0.32	0.34	0.42	0.038	0.42	0.34
D_0	8×10^{-4}		6×10^{-4}	2.5×10^{-2}	2×10^{-4}	8×10^{-4}	6×10^{-4}
	3.5×10^{-3}	1×10^{-2}	1.6×10^{-3}	1.3×10^{-2}	3.7×10^{-4}	3.6×10^{-3}	9.6×10^{-4}
Pd							
E_d	0.71	0.61	0.28	0.42	0.031	0.37	0.33
	0.74	0.59	0.30	0.34	0.059	0.41	0.37
D_0	1.2×10^{-3}		4×10^{-4}	3.3×10^{-2}	5×10^{-4}	1.2×10^{-3}	8×10^{-4}
	6.0×10^{-3}	3×10^{-2}	3.5×10^{-3}	2.4×10^{-2}	4.5×10^{-4}	3.1×10^{-3}	2.0×10^{-3}
Pt							
E_d	0.44	0.31	0.25	0.43	0.007	0.43	0.28
	1.25	0.64	0.53	0.68	0.078	0.63	0.54
D_0	8×10^{-4}		4×10^{-4}	7×10^{-3}	1.0×10^{-4}	8×10^{-4}	6×10^{-4}
	5.0×10^{-3}	1×10^{-2}	1.4×10^{-3}	1.5×10^{-2}	3.5×10^{-4}	2.8×10^{-3}	8.5×10^{-4}

noted that the E_d value for Ni(111) is a rough estimate based upon onset temperature measurements [10].

Table 3 shows that both the AFW and VC results are in excellent agreement with the reanalyzed (see appendix) FIM data for Ni on the (100), (110), (311), and (331) surfaces. However, the calculated activation energy for the Ni(111) surface differs from the experimental value by one order of magnitude.

The FIM results for Pt, Al, and Rh, the only other fcc metals on which self-diffusion has been studied, have been entered into table 4. The only theoretical results given for Rh derive from the Lennard-Jones and Morse potentials, since no high-quality EAM potential exists for Rh. The values of E_d and D_0 are consistent with both the Pt and Al EAM results for most of the crystal faces. Still, the EAM barrier heights are lower than FIM measurements, by as much as a factor of three. For Pt, the VC potential gives better agreement than the AFW potential.

The cross-channel diffusion on the (110) surface for Ni and Pt has been observed in FIM experiments [8–10]. The present EAM study favors the exchange mechanism proposed by Bassett and Webber [44] and later refined by Halicioglu and Pound [45], but with a little difference as depicted in fig. 3. An adatom is most likely to diffuse along the surface channel, since it requires a slightly lower activation energy. In this case the adatom jumps from one potential site to an adjacent one along the channel. An adatom also can jump in the direction perpendicular to the channel, if it gains enough energy. Here, the adatom replaces a wall atom and the wall atom subsequently moves to an adjacent potential minimum, as shown in fig. 3. Note that there are two saddle points along this exchange pathway, with a shallow local minimum (< 0.06 eV) at the symmetric geometry. This agrees with previous observations using Lennard-Jones potentials [46].

The search for an in-channel stationary point with one imaginary frequency was unsuccessful using the VC potential for Al(110). It appears that for this VC potential, the cross-channel exchange saddle lies lower than the in-channel saddle. Consequently, in-channel diffusion occurs via the same saddle point as for cross-channel diffusion. The E_d values obtained for diffusion along the channel

Table 3
Activation energy E_d and the pre-exponential factor D_0 for surface self-diffusion of Ni. E_d is in eV and D_0 is in cm^2/s. The Lennard-Jones values were computed using the Rh potential in ref. [42] and scaled for Ni with the parameters in ref. [43]

Surface	Exp. [10]	Exp. [a]	EAM(AFW)	EAM (VC)	L-J	Morse [17]
(100)						
E_d	0.63		0.63	0.68	0.80	0.29
D_0			1.6×10^{-3}	5.4×10^{-3}	6.9×10^{-3}	
$(110)_{\parallel}$						
E_d	0.23	0.45	0.44	0.39	0.96	0.02
D_0	1×10^{-9}	1×10^{-3}	2.3×10^{-3}	4.0×10^{-3}	8.5×10^{-3}	
$(110)_{\perp}$						
E_d	0.32	0.45	0.49	0.42	1.02	
D_0	1×10^{-7}	1×10^{-3}	3.7×10^{-2}	2.8×10^{-2}	1.0×10^{-1}	
(111)						
E_d	0.33		0.056	0.063	0.15	0.02
D_0			5×10^{-4}	6.2×10^{-4}	9.0×10^{-4}	
(311)						
E_d	0.30	0.37	0.34	0.38	0.50	0.21
D_0	2×10^{-6}	1×10^{-3}	1.4×10^{-3}	4.4×10^{-3}	5.8×10^{-3}	
(331)						
E_d	0.45	0.45	0.45	0.46	1.01	0.15
D_0	2×10^{-3}	1×10^{-3}	1.4×10^{-3}	4.2×10^{-3}	7.9×10^{-3}	

[a] Reanalyzed data.

and across the channel are very similar for Ni, Pt, and Al, in qualitative agreement with experiment. The calculated E_d (0.49 and 0.42 eV) for the Ni(110) cross-channel diffusion are very close to the experimental value (both 0.45 eV). However, the E_d computed for Pt (0.43 eV and 0.68 eV) and Al (0.30 eV and 0.15 eV) differ from the experimental values of 0.76 eV (for Pt) and 0.43 eV (for Al) by up to a factor of 3.

The exchange diffusion mechanism on fcc(100) (see fig. 4) was recently proposed by Feibelman [47,48] based on local density calculations for Al. If an adatom on a (100) surface diffuses exclusively by this mechanism, it executes a random

Table 4
Activation energy E_d and pre-exponential factor D_0 for Pt, Al and Rh. E_d is in eV and D_0 is in cm^2/s. Except where noted, the experimental values for Pt are from ref. [8], Al are from ref. [15], and Rh are from ref. [7]. The Lennard-Jones results were computed using the Rh potential in ref. [42] and scaled for Pt and Al using the parameters in ref. [43]. The Morse results for Pt are from ref. [8]. The Morse Pt results in parentheses and the Rh values are from ref. [17]

Element	Surface		Exp.	EAM(AFW)	EAM(VC)	L-J	Morse
Pt	(100)	E_d		0.44	1.25	1.05	0.82
		D_0		8×10^{-4}	5.0×10^{-3}	4.9×10^{-3}	
	$(100)_{ex}$	E_d	0.47 [48,49]	0.31	0.64	3.97	
		D_0	1.3×10^{-3} [49]		1×10^{-2}	4×10^{-2}	
	$(110)_{\parallel}$	E_d	0.84	0.25	0.53	1.26	0.64 (0.58)
		D_0	8×10^{-3}	4×10^{-4}	1.4×10^{-3}	6.0×10^{-3}	
	$(110)_{\perp}$	E_d	0.78	0.43	0.68	1.34	1.97
		D_0	1×10^{-3}	7×10^{-3}	1.5×10^{-2}	7.4×10^{-2}	
	(111)	E_d		0.007	0.078	0.19	0.07
		D_0		1×10^{-4}	3.5×10^{-4}	6.3×10^{-4}	
	(311)	E_d	0.69	0.43	0.63	0.65	0.50 (0.50)
		D_0		8×10^{-4}	2.8×10^{-3}	4.0×10^{-3}	
	(331)	E_d	0.84	0.28	0.54	1.33	0.77 (0.63)
		D_0	4×10^{-4}	6×10^{-4}	8.5×10^{-4}	5.5×10^{-3}	
Al	(100)	E_d		0.40	0.46	0.60	
		D_0		2×10^{-3}	1.5×10^{-2}	1.0×10^{-2}	
	$(100)_{ex}$	E_d		0.69	0.25	2.28	
		D_0			4×10^{-2}	9×10^{-2}	
	$(110)_{\parallel}$	E_d	0.43	0.26		0.72	
		D_0		2.3×10^{-3}		1.3×10^{-2}	
	$(110)_{\perp}$	E_d	0.43	0.30	0.15	0.77	
		D_0		6.0×10^{-2}	2.4×10^{-2}	1.5×10^{-1}	
	(111)	E_d		0.074	0.054	0.11	
		D_0		9×10^{-4}	1.6×10^{-3}	1.3×10^{-3}	
	(311)	E_d	0.48	0.20	0.24	0.38	
		D_0		2.0×10^{-3}	6.7×10^{-3}	8.5×10^{-3}	
	(331)	E_d	0.46	0.27	0.24	0.76	
		D_0		2.0×10^{-3}	5.4×10^{-3}	1.2×10^{-2}	
Rh	(100)	E_d	0.88			1.04	0.70
		D_0	1×10^{-3}			6.5×10^{-3}	
	$(110)_{\parallel}$	E_d	0.60			1.24	0.48
		D_0	3×10^{-1}			8.0×10^{-3}	
	(111)	E_d	0.16			0.19	0.05
		D_0	2×10^{-4}			8.4×10^{-4}	
	(311)	E_d	0.54			0.64	0.44
		D_0	2×10^{-3}			5.4×10^{-3}	
	(331)	E_d	0.64			1.31	0.62
		D_0	1×10^{-2}			7.4×10^{-3}	

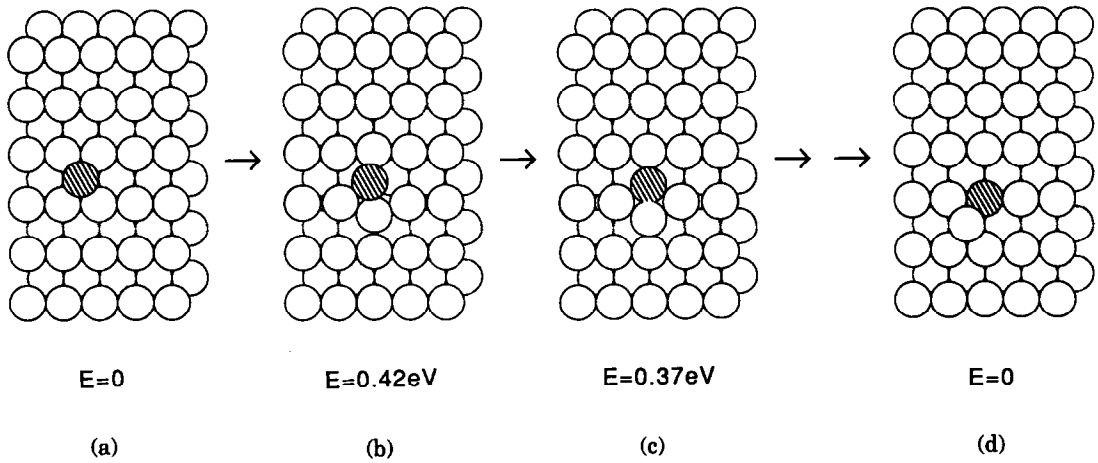

Fig. 3. Ni(110) cross-channel exchange mechanism $\{(110)_{\perp}\}$. Plots and energies are for VC Ni, but 13 of the 14 potentials display the same qualitative behavior: (a) minimum; (b) saddle point; (c) local minimum; (d) minimum. Note that the adatom could just as easily end up one site to the right along the channel. The AFW potential for Pt has only one (symmetric) saddle point.

walk on a $\sqrt{2} \times \sqrt{2}$ square lattice rotated 45° (i.e., the black squares of a checkerboard), so that only half the lattice sites are visited. This rotated visitation lattice was subsequently observed using FIM by Kellogg [48,49] for Pt/Pt(100) and by Chen and Tsong [50] for Ir/Ir(100). It is thus very likely that Pt and Ir undergo exchange diffusion on the (100) surface. The present study shows that only certain metals favor this mechanism. Both the AFW and VC potentials (and the FBD potentials [51]) predict that Pt favors the exchange mechanism, in agreement with experiment. Both sets of potentials also predict that Au and Pd will favor exchange, while the VC potentials additionally predict that Al favors exchange. The $(100)_{ex}$ mechanism seems to offer an exception to the general trend that the E_d values maintain the same ordering with respect to crystal face regardless of the metal. The E_d values for $(100)_{ex}$ swing above and below the E_d values for (100) by as much as 0.5 eV.

The calculated effective vibrational frequencies are between 10^{11} and 10^{13} s^{-1}. These frequencies yield pre-exponential factors of 10^{-4}–10^{-2} cm^2/s, which are in good agreement with experimental values. The similarity of the D_0 values is con-

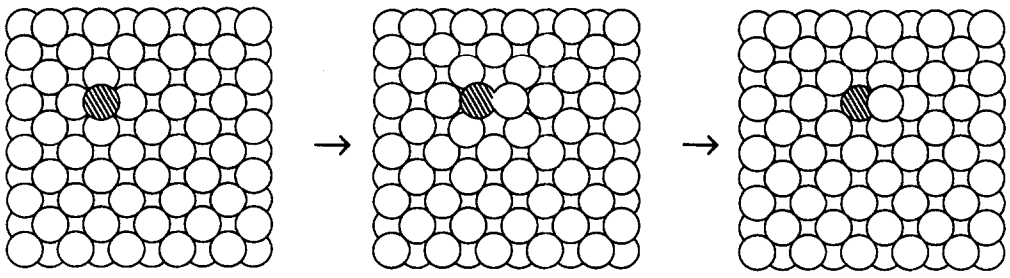

Fig. 4. Pt(100) exchange diffusion mechanism $\{(100)_{ex}\}$. Plots are for VC Pt. This mechanism is favored for Au, Pd and Pt using the AFW potentials and Al, Au, Pd and Pt using the VC potentials.

sistent with the recent clarification made by Wang and Ehrlich [16] concerning the diffusion of Re, W, Mo, Ir, and Rh on the W(211) surface. The values of the pre-exponential factors found with the VC potentials are generally higher than those obtained using the AFW potentials. The VC D_0 values are more reliable because the pre-exponential factors were determined using eq. (6).

The reason for the excellent agreement for Ni [except for Ni(111)] and the poor agreement for Pt and Al between EAM estimates and FIM experimental data is not fully understood. It may be because the band structure of Ni is relatively simple in comparison with other transition metals, making Ni more suitable for the current EAM model. Other studies, such as those that have examined impurity diffusion [22], have suggested that the EAM models are more accurate for Ni than those for Pt. In fact, while the EAM models are quite good for Ni, simple Morse potentials provide better values of the activation energies for Pt. Surface self-diffusion on many of the fcc metals considered in this work (Cu, Ag, Au, and Pd) have not been explored using FIM. Thus, the reliability of our EAM predictions for these metals remains unproven. However, recent EAM calculations of the surface phonons of Cu and Ag [52] are in good agreement with experiment. This may imply that the EAM predictions for surface self-diffusion rates for Cu and Ag are relatively reliable.

For adatoms on the (111) surface of a fcc metal, there are two unique binding sites, corresponding to fcc or hcp stacking of the next layer. These are marked as A (fcc) and B (hcp) in fig. 5. It has been inferred from experiment [10] that there are two different binding sites on Ni(111). Furthermore, Wang and Ehrlich [13] concluded that the hcp site is favored over the fcc in their work on Ir(111). The calculated energy differences between the two sites using the two potentials are very small. The fcc site on the (111) surface is favored using the VC potentials except for Pt, as presented in table 5. For the AFW potentials, the sites are near the cut-off distances of the functions. Hence, it is not proper to predict the extra stability on the (111) surface using the AFW potentials.

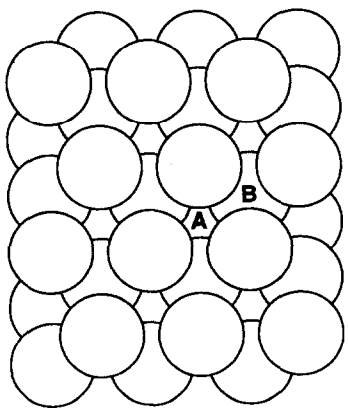

Fig. 5. The two types of adatom binding sites on fcc(111). A = fcc site, B = hcp site.

Table 5
Extra stability of the fcc binding site relative to the hcp site on the fcc(111) surface; the energy differences are given in eV

Metal	$(E_{min}^{hcp} - E_{min}^{fcc})^{VC}$	$(E_{min}^{hcp} - E_{min}^{fcc})^{AFW}$
Ni	0.017	0.002
Cu	0.008	−0.003
Al	0.007	0.002
Ag	0.006	0.000
Au	0.002	0.001
Pd	0.005	0.001
Pt	−0.0007	0.000

5. Conclusions

A systematic study of surface self-diffusion of fcc metals has been performed with the embedded atom method. We draw the following conclusions:

(1) The general trend of the activation energies across the surfaces obtained with the EAM for the fcc metals Cu, Al, Ag, Au, Pd, and Pt is consistent with the experimental observations. The activation energies are the highest on the (100) surfaces (ignoring the exchange mechanism), the lowest on the (111) surfaces, and similar on the (110), (311), and (331) surfaces.

(2) The EAM calculations of the activation energies for Ni [including cross-channel diffusion on the (110) surface] are in excellent agreement with the experimental values for all of the surfaces except the (111). However, the calculated activa-

tion energies for Al and Pt (including cross-channel diffusion on the Pt(110) surface] are lower than the FIM data by as much as a factor of 3.

(3) The exchange mechanism is favored for the (100) surface of Pt, as observed in experiment. The barrier for this exchange mechanism follows a different scaling behavior than the other diffusion mechanisms. It can be lower or higher than the traditional diffusion barrier on the (100) by as much as 0.5 eV.

(4) The EAM potentials yield values of the pre-exponential factor between 1×10^{-4} and 3×10^{-2} cm^2/s, in good agreement with experiment.

(5) Previous EAM calculations of the surface phonons of Cu and Ag match experimental results well. Thus, it is expected that predictions for diffusion rates on these metals are relatively reliable, although no detailed experimental studies for surface diffusion on Cu, Ag, Au, or Pd have been reported.

Acknowledgements

We wish to thank Bill Graham for discussing the reanalysis of his experimental data with us. We also acknowledge Gert Ehrlich, Peter Feibelman, Gary Kellogg, and Michael Cohen for their useful comments. We thank Alan Wright and Murray Daw for sharing their unpublished work with us. We especially appreciate the assistance of Stephen Foiles, Murray Daw, and Mike Baskes in the form of helpful discussions and the sharing of their EAM codes. Two of us (Liu and Adams) would like to thank the National Center for Supercomputing Applications for providing time on their CRAY-XMP. Finally, Liu and Adams thank the Department of Energy for their funding of this program through the Materials Research Laboratory at the University of Illinois, through grant DE-A(O)-76ER01198.

Appendix: reanalysis of surface diffusion data on Ni

The data for Ni are listed separately in table 3 since we have performed a reanalysis of Tung and Graham's experimental data [10]. Their original analysis involved fitting an Arrhenius form to their data. The problem with this approach is that they only had a few data points over a limited temperature range. Thus, small errors in D can translate into large fluctuations in D_0 and E_d. This led to estimates of D_0 ranging over six orders of magnitude. As discussed by Wang and Ehrlich [16], similar large fluctuations in D_0 on the W(211) surface were greatly reduced when D was determined more accurately. Therefore, we reanalyzed Tung and Graham's data by fitting it to an Arrhenius form with $D_0 = 1 \times 10^{-3}$ cm^2/s, a standard value. We discussed this reanalysis with Prof. Graham, and he found it to be a reasonable one. For some surfaces, this yielded a significant change in the value of E_d, as shown in table 3.

References

[1] G. Ehrlich and F.G. Hudda, J. Chem. Phys. 44 (1966) 1039.
[2] D.W. Bassett and M.J. Parsley, J. Phys. D (Appl. Phys.) 2 (1969) 13.
[3] W.R. Graham and G. Ehrlich, Surf. Sci. 45 (1974) 530.
[4] W.R. Graham and G. Ehrlich, Thin Solid Films 25 (1975) 85.
[5] T.T. Tsong, P. Cowan and G.L. Kellogg, Thin Solid Films 25 (1975) 97.
[6] P.L. Cowan and T.T. Tsong, Phys. Lett. A 53 (1975) 383.
[7] G. Ayrault and G. Ehrlich, J. Chem. Phys. 60 (1974) 281; G. Ayrault, PhD Thesis, University of Illinois at Urbana-Champaign (1974).
[8] D.W. Bassett and P.R. Webber, Surf. Sci. 70 (1978) 520.
[9] D.W. Bassett, J. Phys. C (Solid State Phys.) 9 (1976) 2491.
[10] R.T. Tung and W.R. Graham, Surf. Sci. 97 (1980) 73.
[11] T.T. Tsong and G.L. Kellogg, Phys. Rev. B 12 (1975) 1343.
[12] D.A. Reed and G. Ehrlich, Philos. Mag. 32 (1975) 1095.
[13] S.C. Wang and G. Ehrlich, Phys. Rev. Lett. 62 (1989) 2297.
[14] S.C. Wang and G. Ehrlich, Surf. Sci. 224 (1989) L997.
[15] R. Tung, PhD Thesis, University of Pennsylvania (1980).
[16] S.C. Wang and G. Ehrlich, Surf. Sci. 206 (1988) 451.
[17] P.G. Flahive and W.R. Graham, Surf. Sci. 91 (1980) 449.
[18] J.D. Doll and A.F. Voter, Ann. Rev. Phys. Chem. 38 (1987) 413.
[19] M.S. Daw and M.I. Baskes, Phys. Rev. Lett. 50 (1983) 1285.
[20] S.M. Foiles and M.S. Daw, Phys. Rev. B 38 (1988) 12643.
[21] S.M. Foiles and J.B. Adams, Phys. Rev. B 40 (1989) 5909.
[22] J.B. Adams, S.M. Foiles and W.G. Wolfer, J. Mater. Res. 4 (1989) 102.

[23] S.M. Foiles, Surf. Sci. 191 (1987) L779.
[24] A.F. Voter, in: Modeling of Optical Thin Films, Ed. M.R. Jacobson, SPIE 821 (1987) p. 214.
[25] J.A. Rilling, G.M. Gilmore, T.D. Andreadis and J.A. Spraque, Can. J. Phys. 68 (1990) 1035.
[26] M.W. Finnis and J.E. Sinclair, Philos. Mag. A 50 (1984) 45.
[27] F. Ercolessi, M. Parrinello and E. Tosatti, Philos. Mag. A 58 (1988) 213.
[28] S.M. Foiles, M.I. Baskes and M.S. Daw, Phys. Rev. B 33 (1986) 7983.
[29] S.M. Foiles and M.S. Daw, J. Mater. Res. 2 (1987) 5.
[30] A.F. Voter, to be published.
[31] A.F. Voter and S.P. Chen, in: Mater. Res. Soc. Symp. Proc. 82 (1987) 175.
[32] A.F. Voter and J.D. Doll, J. Chem. Phys. 80 (1984) 5832.
[33] C.H. Bennett, in: Diffusion in Solids: Recent Developments, Eds. A.S. Nowick and J.J. Burton, (Academic Press, New York, 1975) p. 73.
[34] J.C. Tully, G.H. Gilmer and M. Shugard, J. Chem. Phys. 71 (1979) 1630.
[35] M.R. Mruzik and G.M. Pound, J. Phys. F (Metal Phys.) 11 (1981) 1403.
[36] G. De Lorenzi and G. Jacucci, Surf. Sci. 116 (1982) 391.
[37] W.M. Franklin, in: Diffusion in Solids: Recent Developments, Eds. A.S. Nowick and J.J. Burton (Academic Press, New York, 1975) p. 1.
[38] S.M. Valone, A.F. Voter and J.D. Doll, Surf. Sci. 155 (1985) 687.
[39] G.H. Vineyard, J. Phys. Chem. Solids 3 (1957) 121.
[40] W.R. Tyson and W.A. Miller, Surf. Sci. 62 (1977) 267.
[41] W.R. Tyson, Can. Met. Q. 14 (1975) 307.
[42] A.F. Voter, Phys. Rev. B 34 (1986) 6819.
[43] T. Halicioglu and G.M. Pound, Phys. Status Solidi A 30 (1975) 619.
[44] D.W. Bassett and P.R. Webber, Surf. Sci. 70 (1978) 520.
[45] T. Halicioglu and G.M. Pound, Thin Solid Films 57 (1979) 241.
[46] G. Jacucci, M. Marchese, G.B. Bachelet, M. Ronchetti, G.L. Chiarotti and G. De Lorenzi, in: Rendiconti della Scuola Internazionale S.I.F. sulla Scienza dei Material, Eds. G.F. Chiarotti, F. Fumi and M.P. Tosi (SIF, Bologna, 1990).
[47] P.J. Feibelman, Phys. Rev. Lett. 65 (1990) 729.
[48] G.L. Kellogg and P.J. Feibelman, Phys. Rev. Lett. 64 (1990) 3143.
[49] G.L. Kellogg, Surf. Sci. 246 (1991) 31.
[50] C. Chen and T.T. Tsong, Phys. Rev. Lett. 64 (1990) 3147.
[51] A.F. Wright and M.S. Daw, private communication.
[52] J.S. Nelson, E.C. Sowa and M.S. Daw, Phys. Rev. Lett. 61 (1988) 1977;
J.S. Nelson, M.S. Daw and E.C. Sowa, Phys. Rev. B 40 (1989) 1465.